Optics Communications 402 (2017) 593–599

Contents lists available at ScienceDirect

Optics Communications

journal homepage: www.elsevier.com/locate/optcom

Three-dimensional kinetic and fluid dynamic modeling and three iterative algorithms for side-pumped alkali vapor lasers

Binglin Shen, Xingqi Xu, Chunsheng Xia, Bailiang Pan *

Department of Physics, Zhejiang University, Hangzhou, 310027, China

ARTICLE INFO

Keywords:
Alkali vapor laser
Side-pumped lasers
Flowed gas
3D temperature distribution

ABSTRACT

Combining the kinetic and fluid dynamic processes in static and flowing-gas diode-pumped alkali vapor lasers, a comprehensive physical model with three cyclically iterative algorithms for simulating the three-dimensional pump and laser intensities as well as temperature distribution in the vapor cell of side-pumped alkali vapor lasers is established. Comparison with measurement of a static side-pumped cesium vapor laser with a diffuse type hollow cylinder cavity, and with classical and modified models is made. Influences of flowed velocity and pump power on laser power are calculated and analyzed. The results have demonstrated that for high-power side-pumped alkali vapor lasers, it is necessary to take into account the three-dimensional distributions of pump energy, laser energy and temperature in the cell to simultaneously obtain the thermal features and output characteristics. Therefore, the model can deepen the understanding of the complete kinetic and fluid dynamic mechanisms of a side-pumped alkali vapor laser, and help with its further experimental design.

1. Introduction

From rubidium vapor [1] to potassium vapor as gain medium [3], from end-pumped configuration [1–4] to side-pumped configuration [5,6], from resonant cavity [1–6] to laser amplifier [7–9], diode-pumped alkali vapor lasers (DPALs) have been under extensive research and development during the past dozen years. Especially since 2010, via the use of high-power diode-pumped and flowing-gas configuration, the output power of DPALs has reached ~kW level [10], demonstrating the potential of DPALs to achieve high efficiency and high power laser. At the same time, quite a lot of theoretical models have been established, including the pioneering model by [11] and other end-pumped models by [12–14], the side-pumped models by [15,16], the kinetic and fluid dynamic models by [17–19], the MOPA (master oscillator power amplifier) models proposed by [20–22] and the XPAL (exciplex pumped alkali laser) models set up by [23].

However, most of these theoretical models only used constant temperature, other recently reported studies have considered the effect of temperature rise [17,18] and the radial temperature profile in the vapor cell [19]. The three-dimensional temperature distribution in end-pumped alkali vapor amplifiers was given by our previous work [22]. But for side-pumped configuration, accurate computational method of the three-dimensional pump intensity and temperature distribution in the whole cell is still absent.

Dominating the distributions of population density of various species of alkali atoms, pump intensity and temperature distribution in the alkali vapor cell influence the output performance of a DPAL a lot, especially for high-power pumped configuration, the steep temperature gradient will stand in the way of realizing a DPAL with high output power. Therefore, after DPALs had stepped into fluid age, it is imperative to study the distributions of the pump and laser energies and temperature in the cell completely. Based on the models of static and flowing-gas end-pumped [17–19] and side-pumped [15] alkali vapor lasers, taking into account the kinetic and fluid dynamic processes, we propose three iterative algorithms and consider more factors to calculate the accurate three-dimensional pump intensity and temperature distribution in the vapor cell. Comparison between the simulation and the experiment of a single-side pumped alkali vapor laser with a cylindrical white diffuse reflector is made, demonstrating the validity of our model. Detailed analysis of the influence of flowed velocity and pump power on output power will be useful for reducing the thermal effects and hence achieving higher output power of the diode-pumped alkali vapor lasers.

2. Computational method for side-pumped alkali vapor lasers

As most of the experiments, the alkali vapor cell is designed into a hollow cylinder with a radius of R and length of L, containing a mix

* Corresponding author.
E-mail address: pbl66@zju.edu.cn (B. Pan).

http://dx.doi.org/10.1016/j.optcom.2017.05.072
Received 17 June 2016; Received in revised form 23 May 2017; Accepted 26 May 2017
0030-4018/

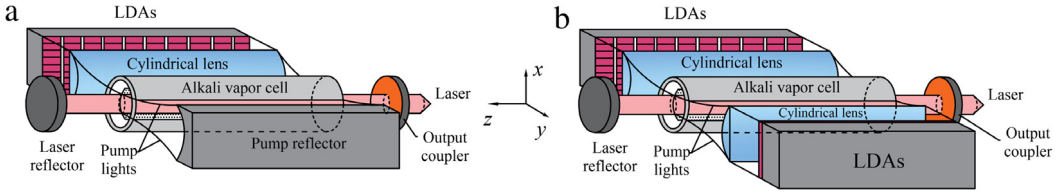

Fig. 1. Schematics of the single-side double-pass (a) and double-side (b) pumped alkali vapor lasers.

of alkali vapor and buffer gases and being housed in a temperature controlled oven. In Fig. 1(a), the pump lights from LDAs (laser diode arrays) are coupled by cylindrical lens into the cell through a slit in the side, and then absorbed by the gain medium as propagating along the y-axis. After that the unabsorbed pump lights will be reflected by the pump reflector for a second pass. In Fig. 1(b), the pump lights from each of the double LDAs are coupled by cylindrical lens through the slits in the same way for a single pass. The resonant cavity consists of a laser reflector and an output coupler.

2.1. Kinetic processes and rate equations

A three-dimension division of the vapor cell as shown in Fig. 2 is made, each divided volume element has dimensions of $dx \times dy \times dz$. For steady-state temperature distribution, the rate equations for the population densities of various species of the alkali atoms in a volume element (xyz) are described as follows:

$$\frac{dn_2(x,y,z)}{dt} = 0 = -W_{21}(x,y,z) + W_{32}(x,y,z) - S_{21}(x,y,z) - Q_{21}(x,y,z) - \sum_{i=4}^{i=6}\left[I_{2i}(x,y,z) + 2Po_{2i}(x,y,z) + Pn_{2i}(x,y,z) - S_{i2}(x,y,z)\right], \tag{1}$$

$$\frac{dn_3(x,y,z)}{dt} = 0 = W_{13}(x,y,z) - W_{32}(x,y,z) - S_{31}(x,y,z) - Q_{31}(x,y,z) - \sum_{i=4}^{i=6}\left[I_{3i}(x,y,z) + 2Po_{3i}(x,y,z) + Pn_{3i}(x,y,z) - S_{i3}(x,y,z)\right], \tag{2}$$

$$\frac{dn_i(x,y,z)}{dt} = 0 = \sum_{j=2,3}\left[I_{ji}(x,y,z) + Po_{ji}(x,y,z) - Pn_{ji}(x,y,z) - S_{ij}(x,y,z)\right] - Ph_i(x,y,z) + b_i R_2^+(x,y,z), \tag{3}$$

$$\frac{dn_{X^+}(x,y,z)}{dt} = 0 = \sum_{i=4}^{i=6} Ph_i(x,y,z) + \sum_{j=2,3}\sum_{i=4}^{i=6} Pn_{ji}(x,y,z) - R^+(x,y,z), \tag{4}$$

$$\frac{dn_{X_2^+}(x,y,z)}{dt} = 0 = R^+(x,y,z) - R_2^+(x,y,z), \tag{5}$$

$$n_1(x,y,z) = N(x,y,z) - \sum_{i=2}^{8} n_i(x,y,z), \tag{6}$$

where X = alkali atom, X^+ and X_2^+ are its ions. n_j ($j = 1,2,3$) and n_i ($i = 4,5,6$) are the respective population densities of the alkali atomic energy levels $n^2S_{1/2}$, $n^2P_{1/2}$, $n^2P_{3/2}$, $n^2D_{3/2}$, $n^2D_{5/2}$ and $(n+2)^2S_{1/2}$, while n_{X^+} and $n_{X_2^+}$ denote the population densities of the X^+ and X_2^+ ions, respectively. The total density $N(xyz)$ in Eq. (6) can be calculated by

$$N(x,y,z) = N_w T_w / T(x,y,z), \tag{7}$$

where $T(xyz)$ obtained in Section 2.4 is the temperature of the volume element, N_w is the total density near the wall and T_w is the wall temperature.

The rates of relaxation W_{32}, spontaneous emission S_{31}, S_{21} and S_{ij}, quenching Q_{j1}, photoexcitation I_{ji}, energy pooling Po_{ji}, photoionization Ph_i, penning ionization Pn and recombination R^+, R_2^+ are given

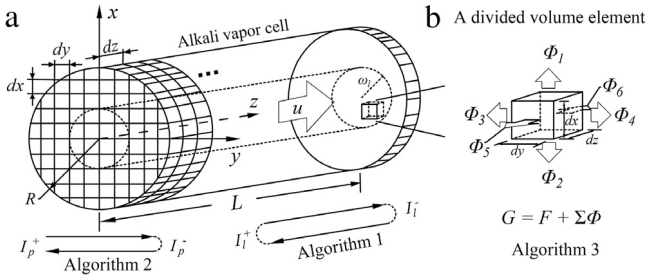

Fig. 2. Schematic illustration of the division procedure of a flowing-gas vapor cell (a) and the conducted heat between a divided volume element and its six neighboring volume elements (b).

by [18,21]. Because the ionizations result in a very small drop in laser power and small density of ions (<2%N) when the pump intensity is less than 20 kW/cm^2 [21] (the maximal pump intensity used in this paper is about 2 kW/cm^2), the movement of ions can be neglected in the rate equations. In addition, due to the recombination and the flow procedure the ions cannot accumulate in the cell. The rates of three-body recombination, two-photon ionization and chemical reactions, as estimated in [17], are negligible and not taken into account. The rates of laser emission W_{21} and pump absorption W_{13} are formulated as

$$W_{21}(x,y,z) = [n_2(x,y,z) - n_1(x,y,z)] \cdot \frac{\sigma_{D1}(x,y,z)[I_l^+(x,y,z) + I_l^-(x,y,z)]}{h\upsilon_l}, \tag{8}$$

$$W_{13}(x,y,z) = \left[n_1(x,y,z) - \frac{1}{2}n_3(x,y,z)\right] \cdot \int \frac{\sigma_{D2}(x,y,z,\lambda)[I_p^+(x,y,z,\lambda) + I_p^-(x,y,z,\lambda)]}{h\upsilon_p} d\lambda, \tag{9}$$

where $\sigma_{D2}(x,y,z,\lambda)$ is the spectrally resolved atomic absorption cross-section and $\sigma_{D1}(x,y,z)$ is the stimulated emission cross-section. $h\upsilon_l$ and $h\upsilon_p$ are the laser and the pump photon energy, respectively. $I_l^{\pm}$ and $I_p^{\pm}$ are the laser and pump intensities which will be discussed specifically in the later subsections.

2.2. Algorithm 1 for longitudinal dimension

In the longitudinal dimension, the laser beam $I_l^{\pm}$ that circulates inside the volume element is coupled out as I_{out} through the output coupler with reflectivity R_{oc}. The main intra-cavity losses include the transmission loss of cell window T_l and the single-pass scattered loss T_s which is assumed to be located at the end of the laser reflector with reflectivity R_l.

Appointing an initial value of output laser power as $P_l \in [0, Pp)$, then the laser intensity on the cross-section of the output end ($z = 0$), which is assumed to have a two-dimensional Gaussian profile, can be described as

$$I_{out}(x,y) = \frac{P_l}{dxdy} \cdot \frac{2dxdy}{\pi\omega_l^2} \exp\left[\frac{-2(x^2+y^2)}{\omega_l^2}\right], \tag{10}$$